

Original citation:

Brunt, Daniel, Balakrishnan, Geetha, Wildes, A. R., Ouladdiaf, B., Qureshi, N. and Petrenko, O. A. (2017) Field-induced magnetic states in holmium tetraboride. *Physical Review B (Condensed Matter and Materials Physics)*, 95 (2). 024410.

Permanent WRAP URL:

<http://wrap.warwick.ac.uk/87972>

Copyright and reuse:

The Warwick Research Archive Portal (WRAP) makes this work by researchers of the University of Warwick available open access under the following conditions. Copyright © and all moral rights to the version of the paper presented here belong to the individual author(s) and/or other copyright owners. To the extent reasonable and practicable the material made available in WRAP has been checked for eligibility before being made available.

Copies of full items can be used for personal research or study, educational, or not-for-profit purposes without prior permission or charge. Provided that the authors, title and full bibliographic details are credited, a hyperlink and/or URL is given for the original metadata page and the content is not changed in any way.

Publisher statement:

© 2017 American Physical Society

A note on versions:

The version presented here may differ from the published version or, version of record, if you wish to cite this item you are advised to consult the publisher's version. Please see the 'permanent WRAP URL' above for details on accessing the published version and note that access may require a subscription.

For more information, please contact the WRAP Team at: wrap@warwick.ac.uk

Field-induced magnetic states in holmium tetraboride

D. Brunt,¹ G. Balakrishnan,¹ A. R. Wildes,² B. Ouladdiaf,² N. Qureshi,² and O. A. Petrenko¹

¹*Department of Physics, University of Warwick, Coventry CV4 7AL, United Kingdom*

²*Institut Laue-Langevin, 6 rue Jules Horowitz, BP 156, 28042 Grenoble Cedex 9, France*

(Received 21 October 2016; revised manuscript received 19 December 2016; published 11 January 2017)

A study of the zero field and field induced magnetic states of the frustrated rare earth tetraboride HoB_4 has been carried out using single crystal neutron diffraction complemented by magnetization measurements. In zero field, HoB_4 shows magnetic phase transitions at $T_{N1} = 7.1$ K to an incommensurate state with a propagation vector $(\delta, \delta, \delta')$, where $\delta = 0.02$ and $\delta' = 0.43$ and at $T_{N2} = 5.7$ K to a noncollinear commensurate antiferromagnetic structure. Polarized neutron diffraction measurements in zero field have revealed that the incommensurate reflections, albeit much reduced in intensity, persist down to 1.5 K despite antiferromagnetic ordering at 5.7 K. At lower temperatures, application of a magnetic field along the c axis initially re-establishes the incommensurate phase as the dominant magnetic state in a narrow field range, just prior to HoB_4 ordering with an *up-up-down* ferrimagnetic structure characterized by the $(h k \frac{1}{3})$ -type reflections between 18 and 24 kOe. This field range is marked by the previously reported $M/M_{\text{sat}} = \frac{1}{3}$ magnetization plateau, which we also see in our magnetization measurements. The region between 21 and 33 kOe is characterized by the increase in the intensity of the antiferromagnetic reflections, such as (100), the maximum of which coincides with the appearance of the narrow magnetization plateau with $M/M_{\text{sat}} \approx \frac{3}{5}$. Further increase of the magnetic field results in the stabilization of a polarized state above 33 kOe, while the incommensurate reflections are clearly present in all fields up to 59 kOe. We propose the H - T phase diagram of HoB_4 for the $H \parallel c$ containing both stationary and transitional magnetic phases which overlap and show significant history dependence.

DOI: [10.1103/PhysRevB.95.024410](https://doi.org/10.1103/PhysRevB.95.024410)

I. INTRODUCTION

In geometrically frustrated systems the competing magnetic interactions lead to a large ground state degeneracy. This suppresses long range order and often results in the formation of unusual ordered phases [1]. Application of a magnetic field can lift the degeneracy and give rise to a rich variety of new magnetic phases and in some notable examples, including garnets [2,3], honeycomb lattices [4,5], and zigzag ladder compounds [6,7], induce long-range order, where none was observed down to the lowest temperatures.

The Shastry-Sutherland lattice (SSL) is an example of a frustrated system with an exact ground state solution. It is a square lattice with antiferromagnetic nearest neighbor interaction J and alternating diagonal antiferromagnetic next nearest neighbor interaction J' [see Fig. 1(a)] [8]. There are only a handful of experimental realizations of this lattice, the most prominent being $\text{SrCu}_2(\text{BO}_3)_2$. One of the most striking features of $\text{SrCu}_2(\text{BO}_3)_2$ are the magnetization plateaus occurring at fractional values of the saturation magnetization M_{sat} . These appear at $M/M_{\text{sat}} = \frac{1}{8}$, $\frac{1}{4}$, and $\frac{1}{3}$ [9,10] and have been suggested to arise due to the localization of a triplet excitation in field [11].

The rare earth tetraborides (RB_4) are another example of the SSL. The RB_4 family crystallizes into a tetragonal structure (space group $P4/mbm$), where the R ions form a network of squares and triangles in the basal plane, which maps to the SSL. The boron atoms form chains of octahedra that run parallel to the c axis. A projection of the ab plane looking along the c axis is shown in Fig. 1(b) [12]. Fractional magnetization plateaus are also a common feature through the series [13–15]. These arise due to a diverse range of magnetic phases stabilized by a magnetic field across the family of compounds, including a ferrimagnetic state

corresponding to $M/M_{\text{sat}} = \frac{1}{2}$ in ErB_4 [16], while TmB_4 has a complex striped structure consisting of regions of antiferromagnetic order, separated by ferromagnetic stripes 7 or 9 units cells apart corresponding to $M/M_{\text{sat}} = \frac{1}{7}$ and $\frac{1}{9}$, respectively. An additional plateau at $M/M_{\text{sat}} = \frac{1}{2}$ arises due to equally sized antiferromagnetic and ferromagnetic stripes [17].

HoB_4 shows successive magnetic phase transitions at $T_{N1} = 7.1$ K and $T_{N2} = 5.7$ K [18]. The magnetic structures of both the low and intermediate temperature magnetic phases have been established by powder neutron diffraction [19]. The intermediate temperature phase (abbreviated to the IT phase in the rest of the paper) was determined to be an incommensurate state with propagation vector $\mathbf{q} = (\delta, \delta, \delta')$, where $\delta = 0.022$ and $\delta' = 0.43$, while the low temperature phase was determined to have noncollinear antiferromagnetic order [19]. Magnetization measurements at $T = 2$ K with a magnetic field applied parallel to the c axis have shown a

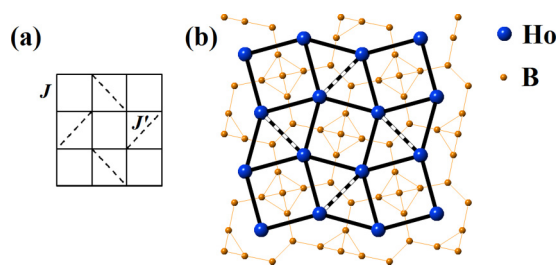


FIG. 1. (a) The Shastry-Sutherland lattice, (b) projection of HoB_4 structure along the tetragonal c axis. The Ho ions form a lattice that topologically maps to the Shastry-Sutherland lattice. Solid bonds correspond to the nearest neighbor interaction J , while the dashed bonds are the next nearest neighbor interaction J' .

plateau at $M/M_{\text{sat}} = \frac{1}{3}$, with further, less pronounced features occurring at $M/M_{\text{sat}} \approx \frac{4}{9}$ and $\frac{3}{5}$ [20]. Significant theoretical work using Heisenberg [21,22] and Ising [23–25] spins has been used to model a variety of members of the RB_4 family with many finding a plateau occurring at $M/M_{\text{sat}} = \frac{1}{3}$, which is experimentally observed in TbB_4 and HoB_4 [20,26]. These models are generally based around the triangles formed by the diagonal J' coupling and include an *up-up-down* structure, in which each triangle has a collinear arrangement of the spins/moments with two of them pointing along the magnetic field and one opposite to it. Another suggestion is an “umbrella” structure where the moments on the triangle are rotated 120° to each other, tilted towards the vertical axis to form a spiral-like structure, which propagates through the lattice [21,25].

A thorough understanding of the field induced behavior in RB_4 is needed to distinguish between different theoretical models describing the magnetization plateaus. In this paper we report the results of our investigation into the nature of the zero-field and field induced magnetic states in HoB_4 using single crystal neutron diffraction as well as complementary magnetization measurements. We find that the IT incommensurate phase “freezes” at low temperature and persists down to at least 1.5 K. For $H \parallel c$, this incommensurate state is also re-established as the dominant magnetic state at lower temperatures for a narrow field range, while the relatively wide $M/M_{\text{sat}} = \frac{1}{3}$ plateau was found to have an *up-up-down* ferrimagnetic state characterized by the $(hk\frac{1}{3})$ -type reflections. We also show that the nature of the much narrower $M/M_{\text{sat}} \approx \frac{3}{5}$ plateau observed in higher fields is completely different, as it is characterized by the reappearance of an in-plane antiferromagnetic component.

The structure of the paper is as follows. The experimental details are described in Sec. II. The experimental results are presented in Sec. III, which is split into two subsections presenting the zero-field polarized neutron diffraction (Sec. III A) and applied field, unpolarized neutron experiments with the additional magnetization measurements (Sec. III B). Finally, we conclude the paper in Sec IV.

II. EXPERIMENTAL DETAILS

Polycrystalline rods of HoB_4 were prepared by arc melting the constituent elements in an argon atmosphere and the floating zone technique was then utilized to grow single crystals. Isotopically enriched boron ^{11}B (99%) was used to reduce neutron absorption. The crystals were checked and aligned using a backscattering x-ray Laue system.

Neutron diffraction measurements were performed at the Institut Laue-Langevin, Grenoble, France. Polarized neutron diffraction experiments were carried out using the D7 instrument [27]. D7 is a cold neutron diffuse scattering spectrometer equipped with xyz polarization analysis. It has three banks of 44 3He detectors, which cover an angular range of approximately 132° . The sample (1.6 g) was fixed to an aluminum holder defining the horizontal $(h0l)$ scattering plane. We used a wavelength of 4.8 Å, which gave a Q -range coverage of 0.09 to 2.5 Å $^{-1}$. Scans were made by rotating the sample around the vertical axis with a 1° step size. Quartz was

used to normalize the polarization efficiency, while vanadium was used to normalize the detector efficiency of the instrument.

Single crystal neutron diffraction in an applied magnetic field was carried out using the D10 diffractometer. A two-dimensional 80×80 mm 2 area detector was used for all measurements [28]. An asymmetric cryomagnet with vertical opening of $+20^\circ$ and -5° supplying a magnetic field of up to 60 kOe was used throughout the experiment. The sample (0.33 g) was fixed to an aluminum holder and the magnetic field was applied along the vertical c axis defining the horizontal $(hk0)$ scattering plane. The accuracy of the alignment of the c axis of the crystal along the magnetic field was better than 0.7° . Incident wavelength of $\lambda = 2.36$ Å and $\lambda = 1.26$ Å from a pyrolytic graphite (PG) and Cu(200) monochromator, respectively, were utilized. The shorter wavelength was utilized in order to reach the out of scattering plane incommensurate reflections. A PG filter was used to reduce contamination of $\lambda/2$. The field and temperature scans were performed by measuring the peak intensity while ramping the field/temperature. The integrated peak intensity was found by summing the counts in a small area of the detector surrounding the reflection. Magnetic refinements of the magnetic phases were carried out using the FULLPROF suite [29].

A Quantum Design SQUID magnetometer was used to measure magnetic susceptibility $\chi(T)$ and an Oxford Instruments vibrating sample magnetometer for the field dependent magnetization. Susceptibility measurements showed a broad maximum at $T_{N1} = 7.1$ K and a small discontinuous drop at $T_{N2} = 5.7$ K, consistent with previous measurements [19]. However, in fields below 1 kOe, there is an additional weak feature visible at $T_C = 15$ K for the crystal used in the D10 experiment. This has been attributed to the ferromagnetic transition in a small HoB_2 impurity [30]. No feature in $\chi(T)$ nor depolarization of the neutron beam was observed for the crystal used during the D7 experiment suggesting the ferromagnetic impurity was insignificant for this sample.

III. RESULTS AND DISCUSSION

A. Polarized neutron measurements

Figure 2 shows the zero-field intensity maps of the $(h0l)$ scattering plane of HoB_4 . For these maps a z polarization was used, which coincided with the vertical $[010]$ axis. Two independent channels were measured, here called the non-spin-flip (NSF) and the spin-flip (SF) channel. The NSF channel is sensitive to nuclear scattering and scattering from a component of the magnetic moment parallel to the neutron polarization, while the SF channel is only sensitive to the component of the magnetic moment in the scattering plane and perpendicular to the scattering vector Q . Hence, the sum of the NSF and SF channels gives the total intensity that would be observed in an unpolarized neutron experiment. In addition there is a small degree of “leakage” between the two channels arising from imperfect polarization of the neutron beam. Although this is corrected for by normalizing to a quartz sample, the correction does not work perfectly for high-intensity Bragg peaks giving rise to a small systematic error corresponding to the exact positions of nuclear Bragg peaks. A comparison of the intensity shows these features are

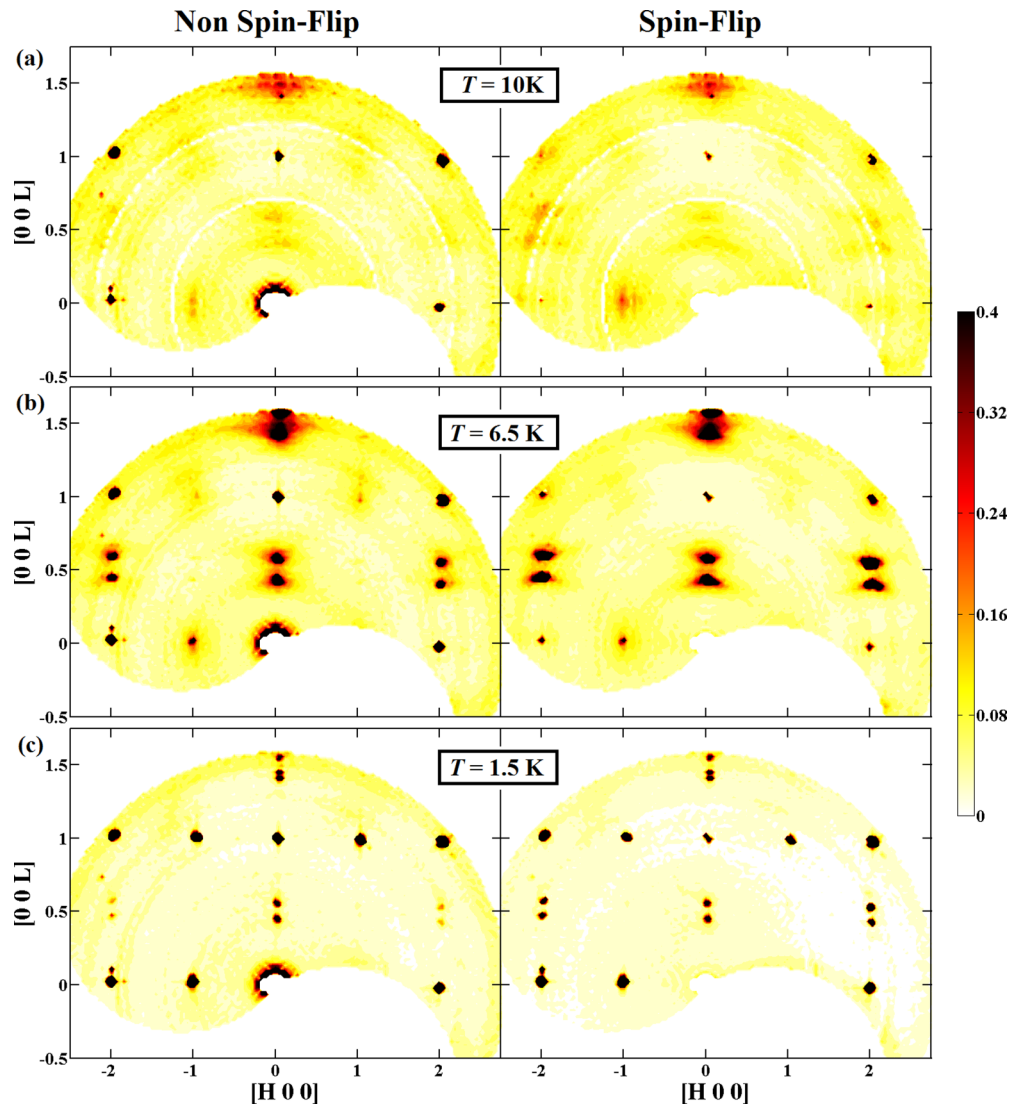


FIG. 2. Single crystal neutron diffraction maps of $(h0l)$ plane for HoB_4 measured using the D7 diffractometer. The non-spin-flip (left column) and spin-flip (right column) channels at different temperature are shown: (a) 10 K, paramagnetic phase, (b) 6.5 K, IT incommensurate phase, and (c) 1.5 K, low-temperature antiferromagnetic phase.

approximately 1% of the intensity of the NSF counterparts and are easily distinguished from real features.

The paramagnetic phase at $T = 10$ K, close to the first magnetic transition, is shown in Fig. 2(a). The nuclear Bragg reflections are observed in the NSF channel, while the weak leakage features are observed in the SF channel. Broad magnetic features are observed around $(0\ 0\ 0.43)$, $(0\ 0\ 1.43)$, $(2\ 0\ 0.43)$, and $(2\ 0\ 1.43)$ corresponding to the positions of incommensurate reflections appearing at lower temperatures. The first transition occurs at $T_{N1} = 7.1$ K and this is diffuse scattering arising from short-range correlations occurring above ordering. Additional diffuse magnetic features are observed at $(\bar{1}00)$, (100) , $(\bar{1}01)$, and (101) . Again these arise due to short-range correlations forming before the onset of long range antiferromagnetic order.

Figure 2(b) shows the IT phase, with an incommensurate propagation vector of $(\delta, \delta, \delta')$, where $\delta = 0.02$ and $\delta' = 0.43$. Although we are unable to resolve $\pm\delta$ separately using D7, we found this to be the propagation vector with the unpolarized

neutron measurements on the D10 diffractometer (see below, Sec. III B). We see a dramatic increase in the intensity of broad features at positions predicted by this propagation vector in both the NSF and SF channels.

This suggests that there is a component of the magnetic moment in the horizontal $(h0l)$ scattering plane as well as one parallel to the $[010]$ direction and is consistent with the proposed incommensurate magnetic structure [19], which is described in more detail in Sec. III B. Additionally we see the appearance of weak features at $(\bar{1}00)$, (101) , and $(\bar{1}01)$ positions in the reciprocal space. These reflections are associated with the commensurate antiferromagnetic structure properly formed in the low temperature phase below $T_{N2} = 5.7$ K, which is starting to appear at intermediate temperatures.

The low temperature phase [Fig. 2(c)] shows a large increase in the intensity of the (100) reflection associated with the antiferromagnetic order as well as an increase in the intensity of all the other commensurate reflections indicating a $\mathbf{q} = 0$ antiferromagnetic structure. Surprisingly we also see

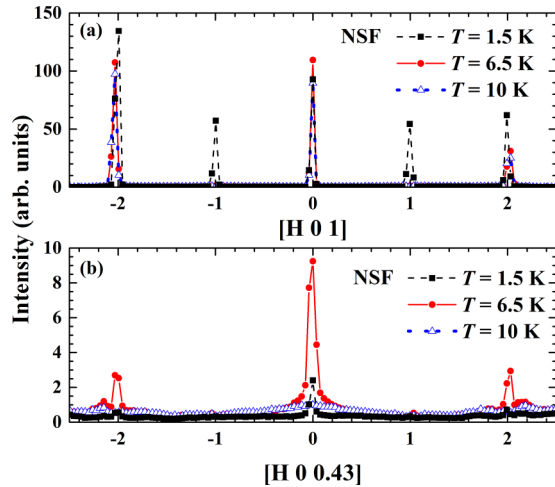


FIG. 3. Line of cuts of the z polarization intensity maps at 10, 6.5, and 1.5 K for the $[H 0 L]$ direction, where (a) $L = 1.0 \pm 0.1$ and (b) $L = 0.43 \pm 0.10$.

the incommensurate reflections persist down to the lowest experimentally available temperature, 1.5 K, although with reduced intensity.

We have taken line cuts through the reciprocal space maps along the $[H 0 L]$ direction for the NSF channel, where $L = 0.43 \pm 0.10$ and 1.0 ± 0.1 to illustrate the temperature evolution of the scattering patterns.

Figure 3(a) showing the cuts along $[H 0 1]$ reveals an increase in intensity of the Bragg peaks between the paramagnetic and IT phases, with a further increase on the (201) and $(\bar{2}01)$ reflections in the low temperature phase. However, there is a decrease in the intensity of the (001) peak between 6.5 and 1.5 K suggesting that this peak is associated with the incommensurate magnetic structure and explains its presence in the SF channel at 1.5 K.

Figure 3(b) showing the line cut $[H 0 0.43]$ shows three peaks at the incommensurate positions. A broad diffuse scattering feature centered on $(0 0 0.43)$ is clearly seen at 10 K. At 6.5 K we see a well defined peak form on top of the diffuse scattering. This two component aspect of the peak suggests there is some disorder associated with the incommensurate phase, which is consistent with previous measurements [19]. However, we observe at 1.5 K the peaks persisting, with reduced intensity, and the diffuse scattering has disappeared. This can also be seen in the intensity maps (Fig. 2) where the broad features are well defined on cooling from 6.5 to 1.5 K in both the NSF and SF channels. We therefore suggest that the remnant intensity arises due to the incommensurate magnetic structure becoming frozen at low temperatures.

B. Applied field measurements

Figure 4 shows the magnetic susceptibility in different fields. The susceptibility curve at $H = 1$ kOe exhibits a broad maximum at $T_{N1} = 7.1$ K and a discontinuous drop at $T_{N2} = 5.7$ K, reflecting the first-order nature of the phase transition between the IT and the low-temperature magnetic structures [19].

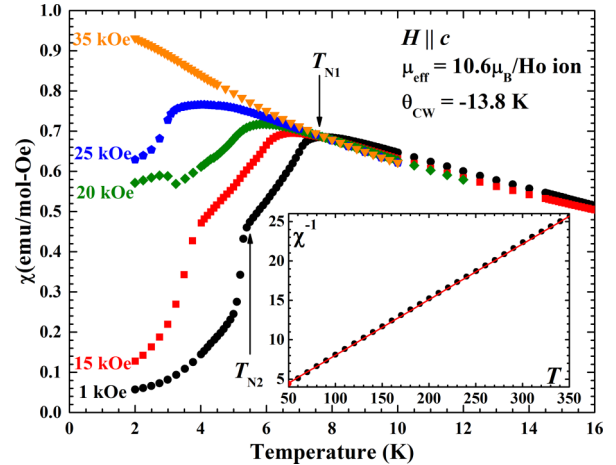


FIG. 4. Temperature dependent magnetic susceptibility in increasing fields applied along $H \parallel c$. Zero-field transition temperatures are indicated by the arrows. The inset shows the inverse susceptibility for $H = 1$ kOe.

The inverse susceptibility shows Curie-Weiss behavior for $T > 50$ K. The effective magnetic moment was determined to be $\mu_{\text{eff}} = 10.6\mu_B$ per Ho ion and the Curie-Weiss constant $\theta_{\text{CW}} = -13.8$ K. These are all in agreement with previously published results [18]. Increasing the field suppresses the ordering temperature and T_{N2} is no longer present above 20 kOe, while T_{N1} persists up to at least 25 kOe.

Figure 5 compares the intensity of fractional $(2.02 1.02 0.43)$, $(hk \frac{1}{3})$ and integer (hkl) reflections with the field dependent magnetization curve at $T = 2$ K. Field dependent neutron and magnetization measurements were performed by ramping the magnetic field up and down, however for clarity (unless stated otherwise) only results where the field was ramped up are shown. The magnetization curve shows a wide plateau at $M/M_{50\text{kOe}} = \frac{1}{3}$, with two smaller features (best seen as local minima in the derivative of the magnetization) occurring at $M/M_{50\text{kOe}} \approx \frac{1}{6}$ and $\frac{3}{5}$. The $\frac{1}{3}$ and $\frac{3}{5}$ have been observed in previously published results [18,20], while the feature at $M/M_{50\text{kOe}} \approx \frac{1}{6}$ has not been observed previously. The magnetization saturates at approximately $6.5\mu_B$ per Ho ion, which is significantly smaller than $10\mu_B$, the predicted saturation moment for a Ho^{3+} ion. It is presently unclear at what strength of an applied field the magnetization will reach the value corresponding to the full polarization of the magnetic moment.

Throughout this section the magnetic states will be referred to as either stationary states, where the magnetization remains almost constant with increasing field or transitional states, where there is a rapid change in the magnetization. The stationary magnetic phases observed in HoB_4 are labeled in Fig. 5 by roman numerals from I to IV. Phase I corresponds to the long range noncollinear antiferromagnetic order, found in the zero field. The field dependence of the antiferromagnetic (100) reflection shows a sharp decrease in intensity at 16 kOe coupled with a sharp increase in the intensity of the incommensurate $(2.02 1.02 0.43)$ reflection, as the antiferromagnetic order gives way to the incommensurate magnetic state in a transitional state between phases I and II. In this transitional

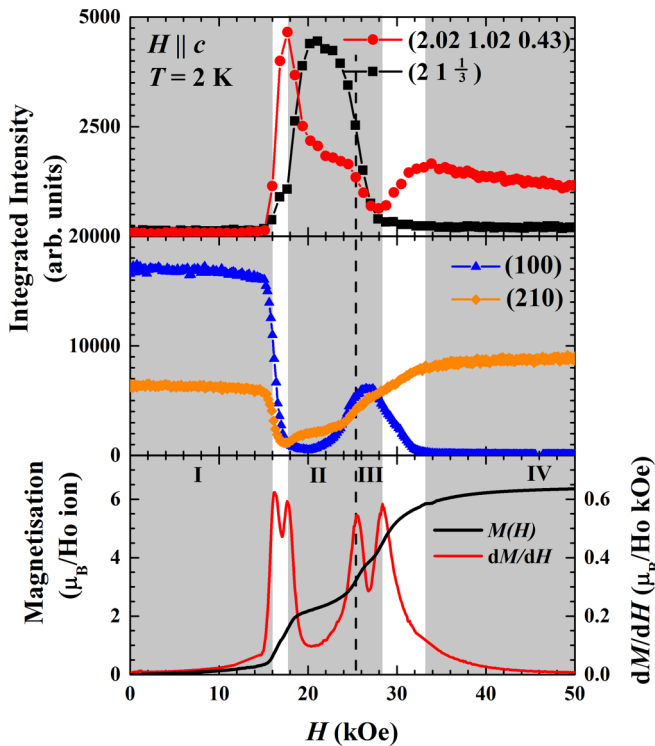


FIG. 5. Evolution of (top panel) fractional and (middle panel) integer (hkl) reflections intensities with magnetic field compared to (bottom panel) the magnetization curve for the magnetic field ramping up at $T = 2$ K. There are four *stationary* magnetic structures, colored in gray and labeled as phases I, II, III, and IV, in which magnetization remains almost constant, while the white regions are *transitional* structures in which magnetization is rapidly changing. The dashed line corresponds to a narrow transitional state between phases II and III.

state, there is also a gradual intensity increase in $(hk\frac{1}{3})$ -type peaks which reach a maximum in phase II, coinciding with the $\frac{1}{3}$ -magnetization plateau. Interestingly the incommensurate reflections persist in phase II as well, although with a reduced intensity. Phase III sees an increase in the (100) reflection, suppressing the incommensurate reflections, suggesting the onset of an antiferromagnetically ordered phase. The region above phase III is a transitory state, where there is a decrease in the intensity of (100) reflection and an increase in both the ferromagnetic (210) and incommensurate reflections up to 33 kOe. The intensity of the ferromagnetic (210) peak plateaus in phase IV and the intensity of the incommensurate reflection gradually decreases with further field increase. The shading used in Fig. 5 emphasises the difference between stationary (gray) and transitional (white) states, while an additional narrow transitional phase between II and III is indicated by a dashed line.

The temperature dependence of the intensity of the $(2.02\ 1.02\ 0.43)$ reflection in different fields is shown in Fig. 6. The zero field data shows the appearance of the $(2.02\ 1.02\ 0.43)$ reflection between $T_{N2} < T < T_{N1}$ corresponding to the incommensurate IT phase. On increasing the field to 10 kOe, the incommensurate phase region shifts to lower temperatures. Increasing further to 20 kOe, which is

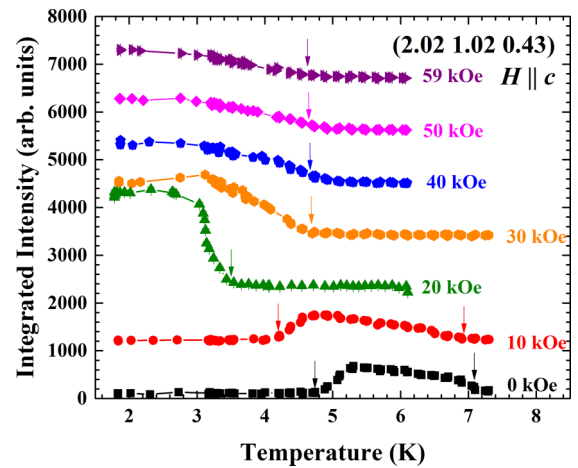


FIG. 6. Temperature dependence of the intensity incommensurate reflection $(2.02\ 1.02\ 0.43)$ in different fields. A stabilization of the incommensurate phase is observed at 20 kOe, while a decrease of the low temperature intensity with increasing field is observed. Each curve is sequentially offset by 1100 counts.

on the tail end of the re-established phase we see a sharp transition with the appearance of the $(2.02\ 1.02\ 0.43)$ reflection at 3.5 K. Increasing the field further up to 59 kOe we see the transition becomes much more gradual, starting at 4.8 K, with the intensity leveling off at approximately 3.2 K. The leveled off intensity at low temperature then decreases with increasing magnetic field. Whether phase IV is an incommensurate phase or a polarized state with a “frozen-in” incommensurate component which is shrinking with increasing field cannot be determined from the present data and further investigation is required.

In the transitional state between phases I and II at $H = 17.5$ kOe we have collected the integrated intensities of a set of 120 incommensurate reflections and performed a magnetic refinements using the model for the zero field incommensurate structure [19]. The fit ($R_{\text{Bragg}} = 15.84\%$) is shown in Fig. 7. We confirmed there was a component of the magnetic moment in the ab plane as well as along the c axis. The moments are tilted from the c axis by approximately 23° compared to 25° degrees reported by Okuyama *et al.* [19] for zero field and the ab plane component points along the [110] direction (see inset Fig. 7). There is an amplitude modulation, which is most prominent along the c axis as a consequence of the propagation vector $(\delta, \delta, \delta')$ being close to commensurate position in the ab plane.

Figure 8 shows the field dependence of the intensity of the $(2\ 1\ \frac{1}{3})$ reflection at different temperatures. The nonzero intensity of this and other symmetry related $(hk\frac{1}{3})$ -type Bragg peaks marks the presence of the phase II coinciding with the $\frac{1}{3}$ -magnetization plateau. With temperature increasing from 1.8 to 4.0 K, the intensity of the $(2\ 1\ \frac{1}{3})$ peak falls dramatically. An increase in the temperature also results in a shift of phase II to a lower field range. In order to determine the magnetic structure of phase II we derived the irreducible representations for a propagation vector of $(0, 0, \frac{1}{3})$. Using a collection of 127 $(hk\frac{1}{3})$ -type reflections, we found the best fit for phase II arises from a basis vector

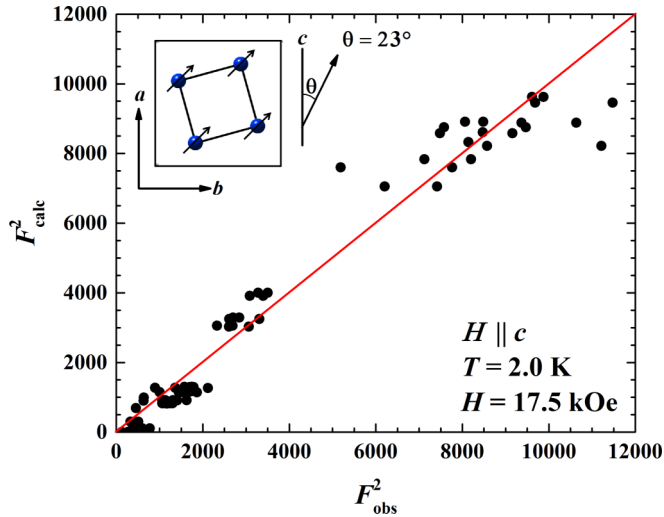


FIG. 7. Comparison of the calculated and observed intensity for the incommensurate phase re-established at $T = 2.0$ K in an applied field of 17.5 kOe. The model for the zero-field incommensurate structure was used to calculate the intensity.

with the moments aligned parallel to c axis. The moments form ferromagnetic layers in the ab plane, which stack in an *up-up-down* arrangement, expanding the crystallographic unit cell along the c axis by a factor of 3. All the moments have equal magnitude with one of the three planes in the unit cell pointing antiparallel compared to the other two layers, thus there is a net magnetization along the c axis which is $\frac{1}{3}$ compared to the full ferromagnetic magnetization. Many of the proposed structures for the $\frac{1}{3}$ and other fractional magnetization plateaus in the RB_4 family involve the arrangement of the magnetic moments only within a single plane of R ions, while the

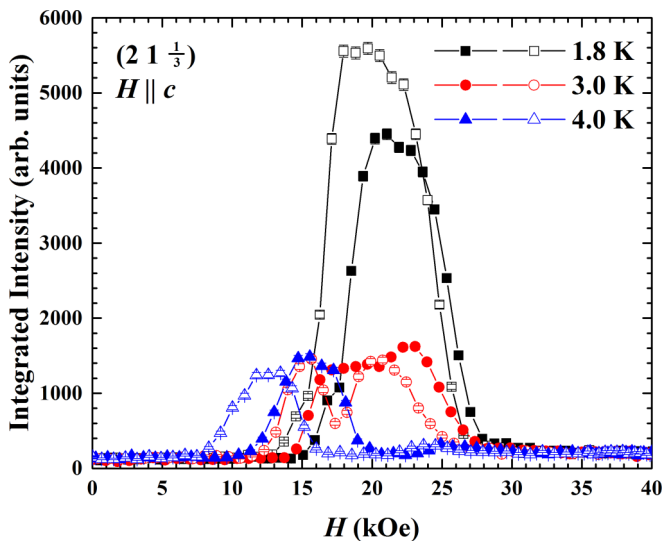


FIG. 8. Field dependence of the intensity of $(2\ 1\ \frac{1}{3})$ reflection at different temperatures. Filled symbols correspond to ramping the field up, empty symbols correspond to ramping the field down. The temperature increase between $T = 1.8$ and 4 K causes a visible shift of the magnetic phase corresponding to $\frac{1}{3}$ -magnetization plateau to lower fields.

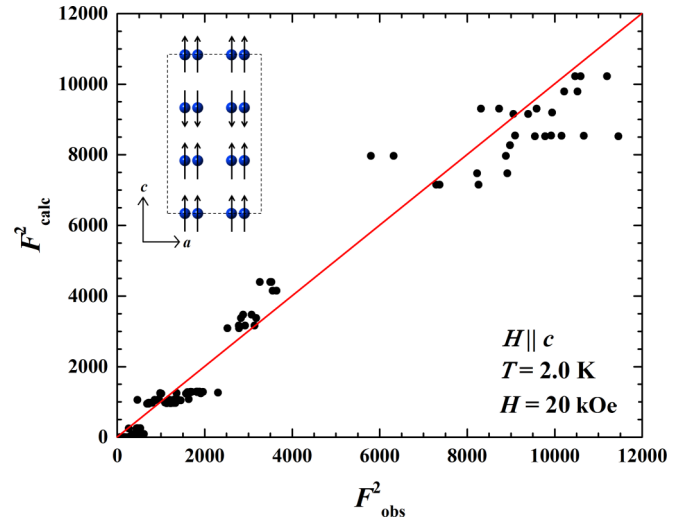


FIG. 9. Comparison of the calculated and observed intensity for phase II corresponding to the $\frac{1}{3}$ -magnetization plateau. An *up-up-down* ferrimagnetic phase along the c axis was used to calculate the intensity. The proposed magnetic structure is shown in the inset.

$\frac{1}{3}$ -magnetization plateau in HoB_4 is clearly caused by the ferrimagnetic stacking of the planes. While there are a number of additional interactions to nearest neighbor and next nearest neighbor are included in these theoretical models (e.g., RKKY interactions, quadrupolar, etc.), with the present results we are unable to clarify the interactions involved in the formation of the UUD structure. The comparison of the observed and calculated intensity for this fit ($R_{\text{Bragg}} = 15.21\%$) is shown in Fig. 9. The refinements gave a c component of the magnetic moment to $1.95\mu_B$ per Ho ion, which is in agreement with the value observed in field dependent magnetization data (Fig. 5). However, this observation does not rule out the presence of a significant magnetization component orthogonal to the c axis both in phase II and phase IV.

As can be seen in Fig. 5, the (100) reflection present at low temperature in lower fields (phase I) initially disappears in an applied field of about 16 kOe and then it is re-established in higher fields (phase III) with a maximum intensity seen around 27 kOe. This reflection is not allowed by the tetragonal crystal symmetry and its presence indicates an antiferromagnetic ordering. We have attempted a magnetic structure determination of this antiferromagnetic phase and for these purposes have subtracted the high temperature (30 K), zero-field intensity of a full collection of integer (hkl) reflections from those at 27 kOe to obtain the purely magnetic intensity. On inspection, the intensity of some reflections, such as the (140) and (330) and their Friedel pairs, has actually decreased on cooling down to base temperature and increasing the field to 27 kOe, therefore the subtraction returned a negative intensity for them. Due to a significant net magnetization in this field we would expect the intensity of the (140) and (330) to either remain constant or for there to be an increase. The observed decrease in intensity could be due to a structural phase transition. In order to test this hypothesis we applied a small distortion to the atoms in the unit cell, assuming the same symmetries. For more information please refer to the Supplemental Material [31]. We found a

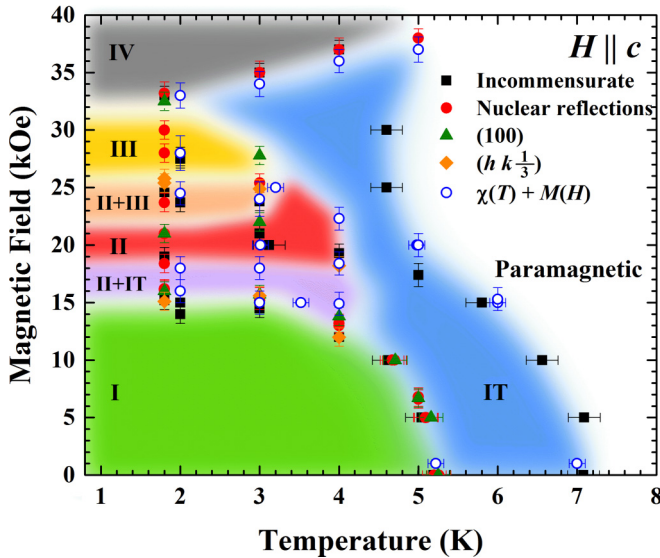


FIG. 10. Magnetic phase diagram of HoB_4 constructed from neutron diffraction data for different reflections (squares, filled circles, triangles, and diamonds) and magnetization (empty circles) measurements. All field dependent measurements were made by ramping the field up. The labeling of different magnetic structures is consistent with the one used in Fig. 5 for $T = 2$ K, however, with the increased temperature the magnetic phases tend to overlap. The separation between the stationary and transitional phases also becomes less obvious on heating, with the *transitory* phases II+IT and II+III occupying large portions of the phase diagram.

displacement of the Ho ions or a compression/expansion of the B octahedra predicted a decrease in intensity for both the (330) and (140) reflections. Although we are unable to confirm a structural distortion with the current data, it is a possible explanation to the negative intensity observed after the subtraction.

Finally, we have constructed the magnetic phase diagram for $H \parallel c$ using temperature and field dependence of the intensity of different reflections from the single crystal neutron experiment as well as the magnetic susceptibility and magnetization measurements. The phase diagram is shown in Fig. 10. The full set of experimental data used to construct the phase diagram is given in the Supplemental Material [31]. Besides the paramagnetic regime and the IT structure, there are four stationary magnetic phases at low temperatures separated by mixed transitional states. In zero field there are two transitions T_{N1} and T_{N2} leading to an incommensurate magnetic IT state and a noncollinear antiferromagnetic state (phase I), respectively. Application of a magnetic field suppresses both T_{N1} and T_{N2} , while for a narrow field range ($16 < H < 18$ kOe) at low temperatures, the IT incommensurate structure

acts as an intermediary phase between the noncollinear antiferromagnetic phase I and the ferrimagnetic *up-up-down* structure formed in phase II. The magnetic structure of phase III remains undetermined, however the presence of the (100) reflection in the single crystal neutron data indicated that it corresponds to an antiferromagnetic arrangement of the Ho moments in the ab plane. The state above phase III is an intermediary phase, where there is an increase in the intensity of the reflections corresponding to a ferromagnetic phase, suggesting that the moments are tilting towards the magnetic field direction. While phase IV corresponds to a fully polarized phase with a frozen-in incommensurate state.

IV. SUMMARY

We have probed the field induced magnetic states of HoB_4 using single crystal neutron diffraction as well as magnetization measurements. Polarized neutron experiments in zero field have revealed diffuse scattering in the paramagnetic regime, heralding the onset of magnetic order. Line cuts through the incommensurate reflection at $(0\ 0\ 0.43)$ at $T = 6.5$ K have shown the peak consists of two components suggesting some disorder in the incommensurate phase. These incommensurate reflections persist down to 1.5 K where a noncollinear antiferromagnetic state is formed. For a magnetic field applied along the c axis, four stationary phases were found, separated by intermediary states which are established over a narrow field ranges. The noncollinear antiferromagnet established in zero field is present up to 16 kOe before the incommensurate state is re-established as the dominant phase between 16 and 18 kOe. The magnetization curve then shows a plateau at $M/M_{50\text{kOe}} = \frac{1}{3}$, coupled with the appearance of $(hk\ \frac{1}{3})$ -type reflection arising from an *up-up-down* ferrimagnetic structure along the c axis. An antiferromagnetic phase is established between 21 and 33 kOe. Finally, there is a polarized phase with remnants of the incommensurate reflections which persist up to 59 kOe. Whether this is an incommensurate phase or a polarized state with the zero field incommensurate phase frozen, cannot be determined and further high field magnetization measurements would be an interesting extension to this work. We hope this study of the field induced magnetic states of HoB_4 will contribute towards the development of theoretical models to describe the plateaus observed in the RB_4 family.

ACKNOWLEDGMENTS

The authors acknowledge enlightening discussions with Pinaki Sengupta, Stephen Lovesey, Dmitry Khalyavin, Denis Golosov, and Frederic Mila, as well as financial support from the EPSRC, UK, through Grant EP/M028771/1. We also thank T. E. Orton for invaluable technical support.

- [1] A. P. Ramirez, *Annu. Rev. Mater. Sci.* **24**, 453 (1994).
- [2] P. Schiffer, A. P. Ramirez, D. A. Huse, and A. J. Valentino, *Phys. Rev. Lett.* **73**, 2500 (1994).
- [3] O. A. Petrenko, D. M. Paul, C. Ritter, T. Zeiske, and M. Yethiraj, *Physica B* **266**, 41 (1999).

- [4] M. Matsuda, M. Azuma, M. Tokunaga, Y. Shimakawa, and N. Kumada, *Phys. Rev. Lett.* **105**, 187201 (2010).
- [5] R. Ganesh, D. N. Sheng, Y.-J. Kim, and A. Paramakanti, *Phys. Rev. B* **83**, 144414 (2011).
- [6] T. H. Cheffings, M. R. Lees, G. Balakrishnan, and O. A. Petrenko, *J. Phys.: Condens. Matter* **25**, 256001 (2013).

- [7] C. Bidaud, O. Simard, G. Quirion, B. Prévost, S. Daneau, A. D. Bianchi, H. A. Dabkowska, and J. A. Quilliam, *Phys. Rev. B* **93**, 060404 (2016).
- [8] B. S. Shastry and B. Sutherland, *Physica B+C* **108**, 1069 (1981).
- [9] S. Miyahara and K. Ueda, *J. Phys.: Condens. Matter* **15**, R327 (2003).
- [10] H. Kageyama, K. Yoshimura, R. Stern, N. V. Mushnikov, K. Onizuka, M. Kato, K. Kosuge, C. P. Slichter, T. Goto, and Y. Ueda, *Phys. Rev. Lett.* **82**, 3168 (1999).
- [11] S. Miyahara and K. Ueda, *Phys. Rev. Lett.* **82**, 3701 (1999).
- [12] J. Etourneau, J. Mercurio, A. Berrada, P. Hagenmuller, R. Georges, R. Bourezg, and J. Gianduzzo, *J. Less Common Metals* **67**, 531 (1979).
- [13] R. Watanuki, H. Mitamura, T. Sakakibara, G. Sato, and K. Suzuki, *Physica B* **378-380**, 594 (2006).
- [14] F. Iga, A. Shigekawa, Y. Hasegawa, S. Michimura, T. Takabatake, S. Yoshii, T. Yamamoto, M. Hagiwara, and K. Kindo, *J. Magn. Magn. Mater.* **310**, e443 (2007).
- [15] S. Yoshii, T. Yamamoto, M. Hagiwara, S. Michimura, A. Shigekawa, F. Iga, T. Takabatake, and K. Kindo, *Phys. Rev. Lett.* **101**, 087202 (2008).
- [16] F. Pfeiffer, W. Schfer, G. Will, J. Etourneau, and R. Georges, *J. Magn. Magn. Mater.* **14**, 306 (1979).
- [17] K. Siemensmeyer, E. Wulf, H.-J. Mikeska, K. Flachbart, S. Gabáni, S. Mat'as, P. Priputen, A. Efdokimova, and N. Shitsevalova, *Phys. Rev. Lett.* **101**, 177201 (2008).
- [18] J. Y. Kim, B. K. Cho, and S. H. Han, *J. Appl. Phys.* **105**, 07E116 (2009).
- [19] D. Okuyama, T. Matsumura, T. Mouri, N. Ishikawa, K. Ohoyama, H. Hiraka, H. Nakao, K. Iwasa, and Y. Murakami, *J. Phys. Soc. Jpn.* **77**, 044709 (2008).
- [20] S. Mat'as, K. Siemensmeyer, E. Wheeler, E. Wulf, R. Beyer, T. Hermansdrfer, O. Ignatchik, M. Uhlarz, K. Flachbart, S. Gabni, P. Priputen, A. Efdokimova, and N. Shitsevalova, *J. Phys.: Conf. Ser.* **200**, 032041 (2010).
- [21] M. Moliner, D. C. Cabra, A. Honecker, P. Pujol, and F. Stauffer, *Phys. Rev. B* **79**, 144401 (2009).
- [22] L. Huo, W. C. Huang, Z. B. Yan, X. T. Jia, X. S. Gao, M. H. Qin, and J.-M. Liu, *J. Appl. Phys.* **113**, 073908 (2013).
- [23] W. C. Huang, L. Huo, G. Tian, H. R. Qian, X. S. Gao, M. H. Qin, and J.-M. Liu, *J. Phys.: Condens. Matter* **24**, 386003 (2012).
- [24] Y. I. Dublenych, *Phys. Rev. E* **88**, 022111 (2013).
- [25] A. Grechnev, *Phys. Rev. B* **87**, 144419 (2013).
- [26] S. Yoshii, T. Yamamoto, M. Hagiwara, T. Takeuchi, A. Shigekawa, S. Michimura, F. Iga, T. Takabatake, and K. Kindo, *J. Magn. Magn. Mater.* **310**, 1282 (2007).
- [27] J. R. Stewart, P. P. Deen, K. H. Andersen, H. Schober, J.-F. Barthélémy, J. M. Hillier, A. P. Murani, T. Hayes, and B. Lindenau, *J. Appl. Crystallogr.* **42**, 69 (2009).
- [28] C. Wilkinson, H. W. Khamis, R. F. D. Stansfield, and G. J. McIntyre, *J. Appl. Crystallogr.* **21**, 471 (1988).
- [29] J. Rodriguez-Carvajal, *Physica B* **192**, 55 (1993).
- [30] J. Roger, V. Babizhetskyy, T. Guizouarn, K. Hiebl, R. Gurin, and J.-F. Halet, *J. Alloys Compd.* **417**, 72 (2006).
- [31] See Supplemental Material at <http://link.aps.org/supplemental/10.1103/PhysRevB.95.024410> for a description of the distortions applied to the atoms in HoB₄ unit cell and how the nuclear intensity was estimated. Additionally, the temperature and field dependence of the intensity of a variety of (*hkl*) reflections is shown.